ChemComm

ROYAL SOCIETY OF CHEMISTRY

COMMUNICATION

View Article Online
View Journal | View Issue

Open Access Article. Published on 23 September 2022. Downloaded on 4/3/2026 12:57:15 AM.
This article is licensed under a Creative Commons Attribution-NonCommercial 3.0 Unported Licence.

Check for updates

Cite this: *Chem. Commun.*, 2022, **58**, 12098

Received 29th July 2022,
Accepted 22nd September 2022

DOI: 10.1039/d2cc04246k

rsc.li/chemcomm

Metal-to-metal electron transfer in a cyanido-bridged $\{Fe_2Co_2\}$ square complex followed by X-ray diffraction and absorption techniques†

Corine Mathonière,*[ab] Dmitri Mitcov,[a] Evangelia Koumousi,[ab] Daniel Amorin-Rosario,[a] Pierre Dechambenoit,[a] Sadaf Fatima Jafri,‡[c] Philippe Sainctavit,[c] Christophe Cartier dit Moulin,[d] Loic Toupet,[e] Elzbieta Trzop,[e] Eric Collet,[e] Marie-Anne Arrio,[c] Andrei Rogalev,[f] Fabrice Wilhelm[f] and Rodolphe Clérac*[a]

The switching properties of a cyanido-bridged Fe/Co square molecule were investigated by single-crystal X-ray diffraction and X-ray absorption spectroscopy at both Fe and Co K-edges. Combining these two techniques, a complete picture of the thermal-, light- and X-ray-induced metal-to-metal electron transfer is obtained, illustrating the concerted role played by the Fe and Co sites.

Switchable coordination complexes offer the possibility to control by temperature and/or light two or more distinct electronic states based on spin crossover (SCO),[1] metal-to-metal[2] or metal-to-ligand[1] electron transfer (ET) processes. These phenomena involve states with different electronic configurations, which can be thermally and optically manipulated. For characterizing the switching between these electronic states, magnetic susceptibility measurements have been extensively used to gather comprehensive information about the molecular and collective natures of the SCO or ET processes, and about the relaxation dynamics of the photo-induced states.[1] Comparatively, detailed X-ray diffraction studies are less routinely reported even if they provide unique structural information about the molecular and supramolecular reorganizations accompanying the electronic switching. For metal-to-metal ET systems, a full description of the redox states requires combined magnetic and structural studies as function of temperature and irradiation in order to understand the electronic and geometrical modifications at each metal ion as well as their impacts on the crystal packing. In addition to the traditional magnetic susceptibility and single-crystal X-ray diffraction (SCXRD) techniques, X-ray Absorption Spectroscopy (XAS) appears to be the ideal local probe to explore metal-to-metal ET properties. The XAS advantages are well illustrated by the different studies on the photomagnetic Fe/Co Prussian Blue Analogues (PBA).[3] The reported results constitute a direct experimental proof of the ET mechanism in these 3D materials involving a concerted reversible redox process between Fe and Co sites.

Since the discovery of photomagnets in 3D PBA networks and their studies with XAS techniques, several switchable Fe/Co molecules have been isolated.[2] However, only a few reports are dedicated to the investigation of the ET process in these molecular analogues by XAS techniques.[4–7] Amongst them, it is worth highlighting that Oshio *et al.* demonstrate in a Fe/Co square complex that the metal-to-metal ET can also be induced by an incident X-ray beam,[7] playing then the double role of a probe and an excitation during the same experiment as previously observed in a few switchable compounds.[8,9]

In 2011, we reported a cyanido-bridged Fe/Co square complex with the formula $\{[(Tp^*)Fe(CN)_3]_2[Co(bpy^{Me})_2]_2\}(OTf)_2\cdot 2DMF\cdot H_2O$ (with Tp* = tris(3,5-dimethylpyrazol-1-yl)hydroborate, bpy^{Me} = 4,4′-dimethyl-2,2′-bipyridine, OTf = trifluoro-methanesulfonate anion and DMF = dimethylformamide).[10] In solid state, this compound, named hereafter **1**, exhibits a thermally reversible ET conversion centered at 174 K involving a paramagnetic $\{Fe_2^{III}Co_2^{II}\}$ excited state and a diamagnetic $\{Fe_2^{II}Co_2^{III}\}$ ground state. In the paramagnetic state, the Fe and Co electronic configurations are $t_{2g}^5e_g^0$ (strong crystal field, S = 1/2) and $t_{2g}^5e_g^2$ (weak crystal field, S = 3/2),

[a] Univ. Bordeaux, CNRS, Centre de Recherche Paul Pascal, CRPP, UMR 5031, 33600 Pessac, France. E-mail: corine.mathoniere@u-bordeaux.fr, rodolphe.clerac@u-bordeaux.fr
[b] Univ. Bordeaux, CNRS, Bordeaux INP, ICMCB, UMR 5026, 33600 Pessac, France
[c] Institut de Minéralogie, de Physique des Matériaux et de Cosmochimie, CNRS UMR7590, Sorbonne Université, MNHN, 75252 Cedex 5, Paris, France
[d] Institut Parisien de Chimie Moléculaire, IPCM, Sorbonne Université, CNRS, F-75005 Paris, France
[e] Univ. Rennes, CNRS, Institut de Physique de Rennes (IPR) – UMR 6251, F-35000 Rennes, France
[f] ESRF – The European Synchrotron, 38043 Grenoble, France

† Electronic supplementary information (ESI) available: Experimental details, crystal structures of **1**, additional XAS spectra, and crystallographic information files (CIF). CCDC 2182862–2182864. For ESI and crystallographic data in CIF or other electronic format see DOI: https://doi.org/10.1039/d2cc04246k

‡ Present address: Department of Physics, University of Karachi, Karachi, Pakistan.

This journal is © The Royal Society of Chemistry 2022

Open Access Article. Published on 23 September 2022. Downloaded on 4/3/2026 12:57:15 AM.
This article is licensed under a Creative Commons Attribution-NonCommercial 3.0 Unported Licence.

respectively, while in the diamagnetic state, both ions are in the strong field configurations, $t_{2g}^6e_g^0$ (S = 0). At the Co sites, the thermally-induced ET is therefore accompanied by a drastic evolution of the ligand field strength and thus spin state, between weak field/high spin and strong field/low spin. Magnetic measurements also revealed that under white-light irradiation at 10 K, **1** is photoconverted from its diamagnetic to paramagnetic state.[10]

In order to study in more details, the local mechanisms of the ET driven by temperature and light in **1**, detailed SCXRD studies were performed at various temperatures and also after white light irradiation (Tables S1 and S2, ESI†). First, the lattice parameters have been measured from 260 to 80 K and, subsequently, after white light exposition at 80 K (ESI†). On cooling, a continuous and concomitant decrease of the unit cell volume and of the three lattice parameters was observed. The large associated volume contraction ($V_s \simeq 65$ Å^3) is directly related to the thermally induced ET (Fig. S1, ESI†). This thermal contraction echoes the decrease of the metal–ligand bond distances associated with the conversion of the thermally populated paramagnetic $\{Fe_2^{III}Co_2^{II}\}$ complexes into their diamagnetic $\{Fe_2^{II}Co_2^{III}\}$ ground state as observed in the magnetic measurements.[10] It is worth mentioning that only the α angle increases slightly during the ET process due to the associated structural reorganization and a significant sliding of the layers formed by the $\{[(Tp^*)Fe(CN)_3]_2[Co(bpy^{Me})_2]_2\}^{2+}$ complexes (MOV1.gif, ESI†). When a single crystal of **1** is exposed at 80 K to a white light (P = 6 mW cm^{-2}), an expansion of the unit cell parameters is observed (Fig. S1, ESI†) in agreement with the photo-induced ET involving the photo-conversion of diamagnetic $\{Fe_2^{II}Co_2^{III}\}$ complexes into their paramagnetic $\{Fe_2^{III}Co_2^{II}\}$ analogues.[10] It is worthwhile to note that the photo-induced state at 80 K exhibits smaller unit cell parameters than those measured at 240 K as expected in presence of a typical thermal contraction (Fig. S1, ESI†). Finally, complete data collections on a single crystal of **1** were performed at 240 K, 80 K before light exposure and 80 K after 4 hours of white light irradiation (P = 6 mW cm^{-2}). The corresponding crystal structures have all been refined in the $P\bar{1}$ space group (Tables S1 and S2, ESI†). As expected, the structures at 240 and 80 K before irradiation are corresponding to the ones previously reported (Fig. S2 and S3, ESI†).[10] A view of the cationic complex after white light irradiation is shown in Fig. 1 and Fig. S2 (ESI†). A visual comparison between the square complex before and after irradiation at 80 K is also provided in MOV2.gif (ESI†). A closer look at the bond distances reveals that upon irradiation the main structural reorganization at the molecular level is an increase of the average Co–N distance from 1.927 Å in the dark to 2.113 Å after light irradiation (Table S2, ESI†). This manifest structure modification is correlated to the photo-induced ET converting $\{Fe_2^{II}Co_2^{III}\}$ complexes into $\{Fe_2^{III}Co_2^{II}\}$ analogues, and to the associated spin-state change at the Co site. Comparatively, smaller increase of the average Fe–C distance is observed from 1.876 to 1.925 Å. For the $\{Fe_2(\mu\text{-}CN)_4Co_2\}$ square complex shown in Fig. 1, the average Fe···Co distance at 80 K changes from 4.891 to 5.113 Å leading to an overall enhancement of the molecular volume driven by the photo-induced ET. The photo-generated cationic $\{Fe_2(\mu\text{-}CN)_4Co_2\}$ core at 80 K has a slightly different geometry when compared to the one observed at 240 K (Fig. S3 and Table S2, ESI†), likely due to the typical thermal contraction (*vide supra* when discussing the unit cell parameters), while the volume expansion ($\simeq$65 Å^3) due to photoinduced ET is similar to the thermally-induced one (Fig. S1, ESI†). The anisotropic lattice contraction is also responsible for a slightly larger distortion of (i) the N–Co–N bond angles and thus of (ii) the Co coordination sphere at 80 K (Tables S1 and S2, ESI†). Analogously, Fe–C–N and C–Fe–C bond angles have values that deviate by 1–3° from those observed at 240 K (Tables S1 and S2, ESI†). This photocrystallography study shows that the photo-induced ET drives important structural reorganizations, both at the molecular and supramolecular levels. The determination of the single-crystal structure in the photo-induced state is an important contribution for understanding how the metal-to-metal ET process occurs. In that sense, there is thus a strong analogy with SCO complexes and their light-induced spin state trapping.[11]

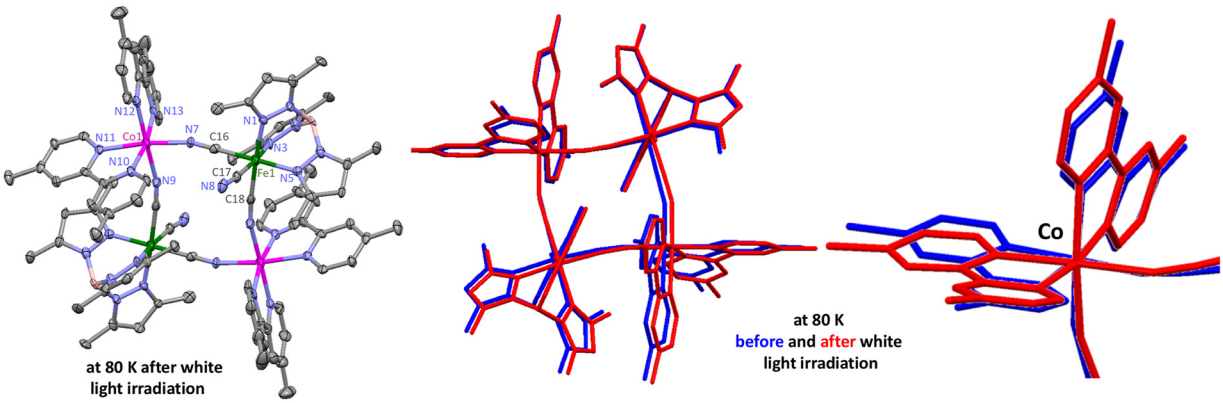

Fig. 1 X-ray crystal structure of the cationic complex in **1** at 80 K after white light irradiation (P = 6 mW cm^{-2}; left). Colour codes: C: grey, N: blue, B: yellow, Fe: green, Co: pink, respectively. Superimposed view of the cationic cores (middle) and Co fragments (right) in **1** showing the differences before (blue) and after (red) white light irradiation at 80 K.

Open Access Article. Published on 23 September 2022. Downloaded on 4/3/2026 12:57:15 AM.
This article is licensed under a Creative Commons Attribution-NonCommercial 3.0 Unported Licence.

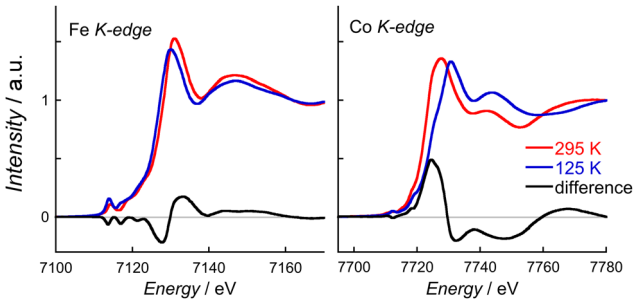

Fig. 2 X-ray absorption spectra (XAS) at 295 K (red) and 125 K (blue), and their difference ($\Delta I_{100\%}$ = I(295 K) − I(125 K); black) for the Fe (left) and Co K-edges (right).

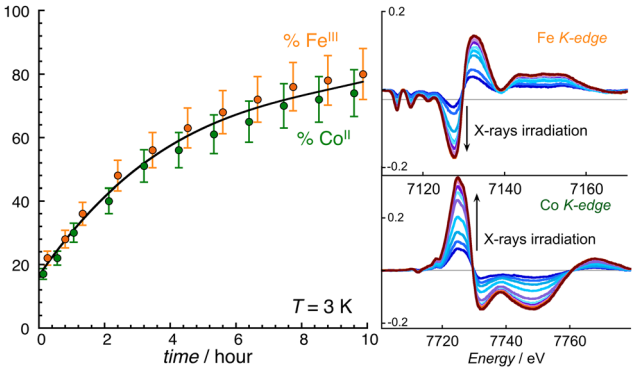

Fig. 3 (Left) Time evolution of the Fe^{III} (orange) and Co^{II} (green) contents in **1** at 3 K during X-ray irradiation (black line: average evolution). The percentages are obtained according to the method described in ESI† (Fig. S7). (right) Evolution of the difference spectra ($\Delta I(t)$ = $I(t)$ − $I(t$ = 0)) during X-ray irradiation.

As shown in the previous paragraph, the ET process is clearly, but indirectly, evidenced by SCXRD techniques through structural modifications of the metal coordination spheres. In order to probe straightforwardly the electronic structures of both metal ions in **1**, XAS measurements at the Fe and Co K-edges have been performed as a function of the temperature. While the main features of the K-edge spectra are due to the 1s → 4p electric dipole transitions, small peaks or shoulders corresponding to the 1s → 3d electric quadrupole transitions are observed at lower energies. This pre-edge region is often used in literature to determine the oxidation and spin states of the metal ions such as Fe or Co.[12] Beyond the simple visual comparison with reference samples, the electronic configuration of a metal ion can be reliably established by comparing the experimental data with the theoretical spectra from Ligand Field Multiplet (LFM) calculations.[13] The theoretical analysis of the pre-edge regions is provided in supplementary materials (ESI†).[14] In agreement with the metal-to-metal ET described in **1** (*vide supra*),[10] both pre-edge and edge regions (Fig. 2, Fig. S4 and S5, ESI†) indicate that the Fe and Co metal ions are respectively reduced (from Fe^{III} to Fe^{II}) and oxidized (from Co^{II} to Co^{III}) when decreasing the temperature from 295 to 125 K.[3b] It is worth noting that the XAS fingerprints of the Co^{II} and Fe^{III} metal ions are completely absent at 125 K suggesting that the thermally induced ET is quantitative. If the overall modification of the Fe K-edge is relatively modest with an 1 eV energy shift, larger variations are measured at the Co K-edge (Fig. 2). Indeed, this reflects well the previously discussed structural analysis that highlights an important shortening of the Co–N bonds at low temperatures and a substantial modification of the Co coordination sphere. When plotting the spectral difference between the 295 and 125 K XAS spectra (Fig. 2), antagonistic features are observed in relation with the complementary roles played by the two metal ions during the ET process. While the Fe difference spectrum shows first negative peaks (at 7128 eV) and then positive peaks around 7133 eV, the reverse signature is observed for Co with first a maximum at 7725 eV and then two minima above 7732 eV.

In order to investigate the potential X-ray sensitivity of **1**, a sample was cooled down to 3 K in the dark and then irradiated with X-rays during 10 hours by collecting continuously and alternatively XAS spectra at Co and Fe K-edges (Fig. 3). The difference spectra, $\Delta I(t) = I(t) - I(t = 0)$, at the respective edges reveal an efficient X-ray induced conversion of the $\{Fe_2^{II}Co_2^{III}\}$ complexes in **1** into their paramagnetic $\{Fe_2^{III}Co_2^{II}\}$ analogues (Fig. 3 and Fig. S6, ESI†). The time evolution of the Fe^{III} and Co^{II} populations (Fig. 3 and Fig. S6, ESI†) can be estimated accurately and independently during the 10 hours of the experiment (Fig. S7, ESI†). The amount of Fe^{III} and Co^{II} sites increases with the irradiation time in a concomitant and identical manner (Fig. 3), attesting the concerted role of the Fe and Co ions in the ET process. After about 10 hours, the conversion of the $\{Fe_2^{II}Co_2^{III}\}$ complexes into their paramagnetic analogues reaches about 80% (Fig. 3), which is consistent with the only similar data on a molecular PBA.[7] Compound **1** shows a complete reversibility and reproducibility of the thermally and X-ray induced ET as demonstrated by the XAS spectra at 250 K and 125 K (Fig. S8, ESI†), which are perfectly superposed to those in the same temperature range before 10 hours of X-ray irradiation. In the used experimental conditions, it is important to highlight the absence of a detectable amount of Fe^{II} or Co^{III} at 250 K, and of Fe^{III} or Co^{II} at 125 K, and thus the lack of X-ray damages for this molecular system.

To further study by XAS the thermally and X-ray induced ET process in **1**, the normalized $\Delta I_{100\%}$ at its maximum value of 7725 eV for the Co K-edge (Fig. 2) was monitored (i) from 230 to 3 K (at 1 K min^{-1}), (ii) during 10 hours of X-ray irradiation (Fig. 3) and finally (iii) from 3 to 240 K (at 1 K min^{-1}). As shown in Fig. 4 (blue trace), the thermally induced ET is clearly detected upon cooling with a $T_{1/2}$ value around 170 K. All these data agree with the bulk magnetic measurements (Fig. S9, ESI†). Below 100 K, a small increase of the XAS signal at 7725 eV from almost 0 is observed to reach a value 0.15 at 3 K. Therefore, 15% of Co^{II}, and thus 15% of $\{Fe_2^{III}Co_2^{II}\}$ complexes, are already X-ray generated in **1** during this cooling experiment realized under continuous X-ray exposure (at 7725 eV). As already discussed above, a subsequent 10 hours irradiation leads to about 80% X-ray induced conversion (Fig. 3). Upon increasing the temperature, the XAS signal at 7725 eV remains first constant up to 80 K, indicating that X-ray

Open Access Article. Published on 23 September 2022. Downloaded on 4/3/2026 12:57:15 AM.
This article is licensed under a Creative Commons Attribution-NonCommercial 3.0 Unported Licence.

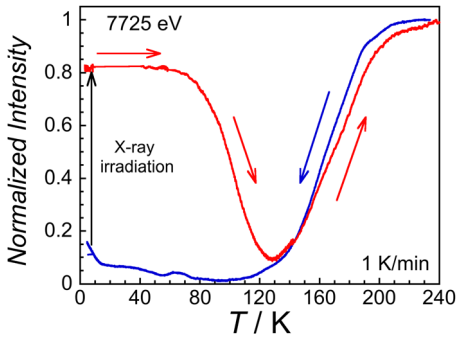

Fig. 4 Temperature dependence of the XAS intensity with a scan rate of 1 K min^{-1} at 7725 eV (Co K-edge) between 230 and 3 K (blue) and between 3 and 240 K (red) after 10 hours of X-ray irradiation at 3 K (black arrow).

induced Co^{II} metals ions stay thermally trapped, and then decreases to a minimum value around 125 K as expected when $\{Fe_2^{III}Co_2^{II}\}$ squares relax to their $\{Fe_2^{II}Co_2^{III}\}$ ground state. Above 125 K, the XAS data follow the cooling process with a good reproducibility of the thermally induced ET (Fig. S9, ESI†).

The foregoing results describe the first complete investigation of the ET process in a cyanido-bridged Fe/Co square complex by combining complementary diffraction and absorption X-ray techniques. The X-ray diffraction studies revealed first the modifications at the macroscopic level of the unit cell parameters during the thermally- and white-light induced ET. The detailed comparison of the crystal structures at 240 K and 80 K before and after white-light irradiation highlighted the key structural features characterizing the reversible switching between $\{Fe_2^{II}Co_2^{III}\}$ and $\{Fe_2^{III}Co_2^{II}\}$ square complexes. In parallel, the use of an attenuated X-ray beam to avoid radiation damage together with a highly efficient X-ray fluorescence detection allowed to record high quality XAS data at the ESRF. The thermally and X-ray induced metal-to-metal ET properties were thus investigated independently at Fe and Co K-edges to probe locally the reversibility and the reproducibility of the intramolecular Fe/Co redox process. The XAS results established without ambiguity the concerted and concomitant reduction/oxidation of the two metal ion partners involved in the ET triggered by temperature and X-ray exposure. This study demonstrates not only the power of the XAS technique to locally study fragile ET and redox-active systems but also confirms its complementarity with more traditional structural, optical and magnetic measurements. Work is now underway to use time-resolved optical and X-ray spectroscopies[11,15] to follow the thermally and photo-induced ET at ultrafast timescales.

The authors thank for technical and financial supports the University of Bordeaux, Sorbonne University, the University of Rennes, the Région Nouvelle Aquitaine, Quantum Matter Bordeaux (QMBx), the CNRS, the Association Française de Magnétisme Moléculaire and the ESRF for the beamtime allocation (CH-4330).

Conflicts of interest

There are no conflicts to declare.

Notes and references

1 M. A. Halcrow, *Spin-Crossover Materials: Properties and Applications*, John Wiley & Sons, 2013.
2 (*a*) D. Aguila, Y. Prado, E. S. Koumousi, C. Mathonière and R. Clérac, *Chem. Soc. Rev.*, 2016, **45**, 203–224; (*b*) M. Nihei, *Chem. Lett.*, 2020, **49**, 1209–1215; (*c*) W. Huang, X. Ma, O. Sato and D. Wu, *Chem. Soc. Rev.*, 2021, **50**, 6832–6870.
3 (*a*) T. Yokoyama, T. Ohta, O. Sato and K. Hashimoto, *Phys. Rev. B: Condens. Matter Mater. Phys.*, 1998, **58**, 8257–8266; (*b*) C. Cartier dit Moulin, F. Villain, A. Bleuzen, M.-A. Arrio, Ph. Sainctavit, C. Lomenech, V. Escax, F. Baudelet, E. Dartyge, J.-J. Gallet and M. Verdaguer, *J. Am. Chem. Soc.*, 2000, **122**, 6653–6658; (*c*) A. Mondal, Y. Li, M. Seuleiman, M. Julve, L. Toupet, M. Buron-Le cointe and R. Lescouezec, *J. Am. Chem. Soc.*, 2013, **135**, 1653–1656; (*d*) S. F. Jafri, M.-A. Arrio, A. Bordage, R. Moulin, A. Juhin, C. Cartier dit Moulin, E. Otero, P. Ohresser, A. Bleuzen and Ph. Sainctavit, *Inorg. Chem.*, 2018, **57**, 7610–7619; (*e*) A. Bordage, R. Moulin, E. Fonda, G. Fornasieri, E. Rivière and A. Bleuzen, *J. Am. Chem. Soc.*, 2018, **140**, 10332–10343.
4 Y. Sekine, M. Nihei, R. Kumai, H. Nakao, Y. Murakami and H. Oshio, *Inorg. Chem. Front.*, 2014, **1**, 540–543.
5 S. F. Jafri, E. S. Koumousi, M.-A. Arrio, A. Juhin, D. Mitcov, M. Rouzières, P. Dechambenoit, D. Li, E. Otero, F. Wilhelm, A. Rogalev, L. Joly, J.-P. Kappler, C. Cartier dit Moulin, C. Mathonière, R. Clérac and Ph. Sainctavit, *J. Am. Chem. Soc.*, 2019, **141**, 3470–3474.
6 (*a*) M. L. Baker, Y. Kitagawa, T. Nakamura, K. Tazoe, Y. Narumi, Y. Kotani, F. Iijima, G. N. Newton, M. Okumura, H. Oshio and H. Nojiri, *Inorg. Chem.*, 2013, **52**, 13956–13962; (*b*) M. L. Baker, S.-Q. Wu, S. Kang, S. Matsuzawa, M.-A. Arrio, Y. Narumi, T. Kihara, T. Nakamura, Y. Kotani, O. Sato and H. Nojiri, *Inorg. Chem.*, 2019, **58**, 10160–10166; (*c*) N. Daffé, J.-R. Jimeńez, M. Studniarek, A. Benchohra, M.-A. Arrio, R. Lescouëzec and J. Dreiser, *J. Phys. Chem. Lett.*, 2019, **10**, 1799–2804.
7 Y. Sekine, M. Nihei, R. Kumai, H. Nakao, Y. Murakami and H. Oshio, *Chem. Commun.*, 2014, **50**, 4050–4052.
8 (*a*) V. Escax, A. Bleuzen, J. P. Itie, P. Munsch, F. Varret and M. Verdaguer, *J. Phys. Chem.*, 2003, **107**, 4763–4767; (*b*) D. Papanikolaou, S. Margadonna, W. Kosaka, S.-i Ohkoshi, M. Brunelli and K. Prassides, *J. Am. Chem. Soc.*, 2006, **128**, 8358–8363; (*c*) T. Yokoyama, K. Okamoto, T. Ohta, S.-I. Ohkoshi and K. Hashimoto, *Phys. Rev. B: Condens. Matter Mater. Phys.*, 2002, **65**, 064438; (*d*) S. Margadonna, K. Prassides and A. N. Fitch, *Angew. Chem., Int. Ed.*, 2004, **43**, 6316–6319.
9 (*a*) G. Poneti, M. Mannini, L. Sorace, Ph. Sainctavit, M.-A. Arrio, E. Otero, C. Criginski and A. Dei, *Angew. Chem., Int. Ed.*, 2010, **49**, 1954–1957; (*b*) G. Vankó, F. Renz, G. Molnár, T. Neisius and S. Kárpáti, *Angew. Chem., Int. Ed.*, 2007, **46**, 5306–5309; (*c*) T. M. Francisco, W. J. Gee, H. J. Shepherd, M. R. Warren, D. A. Shultz, P. R. Raithby and C. B. Pineiro, *J. Phys. Chem. Lett.*, 2017, **8**, 4774–4778.
10 D. Siretanu, D. Li, L. Buisson, D. M. Bassani, S. M. Holmes, C. Mathonière and R. Clérac, *Chem. – Eur. J.*, 2011, **17**, 11704–11708.
11 H. T. Lemke, K. S. Kjær, R. Hartsock, T. B. van Driel, M. Chollet, J. M. Glownia, S. Song, D. Zhu, E. Pace, S. F. Matar, M. M. Nielsen, M. Benfatto, K. J. Gaffney, E. Collet and M. Cammarata, *Nat. Commun.*, 2017, **8**, 15342.
12 (*a*) T. E. Westre, P. Kennepohl, J. G. De Witt, B. Hedman, K. O. Hodgson and E. I. Solomon, *J. Am. Chem. Soc.*, 1997, **119**, 6297–6314; (*b*) M. Lundberg, T. Kroll, S. DeBeer, U. Bergmann, S. A. Wilson, P. Glatzel, D. Nordlund, B. Hedman, K. O. Hodgson and E. I. Solomon, *J. Am. Chem. Soc.*, 2013, **135**, 17121–17134; (*c*) G. Poneti, M. Mannini, L. Sorace, Ph. Sainctavit, M.-A. Arrio, A. Rogalev, F. Wilhelm and A. Dei, *ChemPhysChem*, 2009, **10**, 2090–2095.
13 (*a*) B. T. Thole, R. D. Cowan, G. A. Sawatzky, J. Fink and J. C. Fuggle, *Phys. Rev. B: Condens. Matter Mater. Phys.*, 1985, **31**, 6856–6858; (*b*) F. de Groot and A. Kotani, *Core Level Spectroscopy of Solids*, CRC Press, Boca Raton, 2008.
14 S. F. Jafri, E. S. Koumousi, Ph. Sainctavit, A. Juhin, V. Schuler, O. Bunau, D. Mitcov, P. Dechambenoit, C. Mathonière, R. Clérac, E. Otero, P. Ohresser, C. Cartier dit Moulin and M.-A. Arrio, *Inorg. Chem.*, 2016, **55**, 6980–6987.
15 M. Cammarata, S. Zerdane, L. Balducci, G. Azzolina, S. Mazerat, C. Exertier, M. Trabuco, M. Levantino, R. Alonso-Mori, J. M. Glownia, S. Song, L. Catala, T. Mallah, S. F. Matar and E. Collet, *Nat. Chem.*, 2021, **13**, 10–14.